Acta Crystallographica Section B
Structural Science
ISSN 0108-7681

A time-resolved powder diffraction study of *in-situ* photodimerization kinetics of 9-methylanthracene using a CCD area detector and parametric Rietveld refinement

Ahmed F. Mabied,[a] Melanie Müller,[b,c] Robert E. Dinnebier,[b] Shunsuke Nozawa,[d] Manabu Hoshino,[e,f] Ayana Tomita,[d] Tokushi Sato[d] and Shin-ichi Adachi[a,d,g]*

[a]Department of Materials Structure Science, School of High Energy Accelerator Science (KEK), The Graduate University for Advanced Studies (Sokendai), Tsukuba 305-0801, Japan, [b]Max-Planck-Institute for Solid State Research, Heisenbergstrasse 1, 70569 Stuttgart, Germany, [c]Department of Materials Engineering and Industrial Technologies, University of Trento, Via Mesiano 77, 38123 Trento, Italy, [d]Photon Factory, High Energy Accelerator Research Organization (KEK), Tsukuba 305-0801, Japan, [e]Department of Chemistry and Materials Science, Tokyo Institute of Technology, Meguro-ku, Japan, [f]CREST, Japan Science and Technology Agency (JST), Japan, and [g]PRESTO, Japan Science and Technology Agency (JST), Japan

Correspondence e-mail: shinichi.adachi@kek.jp

Received 24 March 2012
Accepted 17 June 2012

The $[4\pi + 4\pi]$ photodimerization process of the 9-substituted anthracene derivative crystalline 9-methylanthracene (9-MA) was investigated using time-resolved X-ray powder diffraction. The study was carried out *in-situ* using a CCD area detector. Sequential and parametric Rietveld refinement was applied for quantitative phase analysis. The results of traditional sequential Rietveld refinement showed that the evolution of the dimerization process can be described using the Johnson–Mehl–Avrami–Kolmogorov (JMAK) model. The parameters of the JMAK equation were obtained successfully by parametric Rietveld refinement and suggest that the reaction follows heterogeneous nucleation and one-dimensional growth with a decreasing nucleation rate.

1. Introduction

Although single-crystal diffraction is a powerful technique, it is not always suitable for studying the dynamics of solid-state reactions, because either the samples cannot be prepared as single crystals of sufficient size and quality for diffraction studies or the reaction cannot be completed as a result of crystal disintegration (Harris *et al.*, 1994; Turowska-Tyrk & Trzop, 2003). In such cases powder diffraction is the method of choice. Beyond this, the stability and efficiency of kinetic studies of phase transitions by powder diffraction have been recognized (Müller *et al.*, 2009). Furthermore, area detectors (such as CCDs) offer a number of advantages, for example short exposure time, applicability to imperfect powder samples (*e.g.* with preferred orientation and/or large grain size, single-crystal spots *etc.*) and *in-situ* studies (Svensson *et al.*, 1997).

One of the well known solid-state reactions is the photodimerization of organic compounds, which recently has been of interest because of its important applications, such as selective organic syntheses and optical data storage devices (Turowska-Tyrk, 2004; Feringa *et al.*, 2000). The nature of the solid state requires a minimum amount of molecular movements for a reaction to occur. Schmidt (1971) proposed a topochemical rule for solid-state reactions, where the nearest-neighbouring double-bond distance should be around 4.2 Å.

Anthracene derivatives undergo a $[4\pi + 4\pi]$ photodimerization across the 9,10-positions of anthracene rings upon illumination of light at $\lambda > 300$ nm. The dimer phase can be reversed into its initial monomers thermally or by illumination of light at $\lambda < 300$ nm (Bouas-Laurent *et al.*, 2000; Bratschkov *et al.*, 2001) as shown in Fig. 1, which is considered to be a unique property of anthracene derivatives. Hence, a wide variety of applications in different fields was developed, for example light-switched chromic devices (Tsudera *et al.*, 1997), photo-switchable receptors (Molard *et al.*, 2006) and

optical storage memory devices (Dvornikov & Rentzepis, 1996). Further applications such as scintillation counters are well known due to the work of Bell (1948).

Kinetic analysis can be performed by measuring the converted fraction of a material as a function of illumination time (Kim *et al.*, 2003). Recently, kinetic models were reported for $[2\pi + 2\pi]$ and $[4\pi + 4\pi]$ photodimerization in the solid state using the JMAK (Johnson–Mehl–Avrami–Kolmogorov) model (Benedict & Coppens, 2009; Moré *et al.*, 2010).

The fraction of the product (dimer) phase can be obtained accurately by Rietveld quantitative analysis of X-ray powder diffraction data (Madsen & Scarlett, 2008). Stinton & Evans (2007) introduced the parametric Rietveld refinement, which allows all powder patterns to be included in a single refinement. Moreover, the parameters of the JMAK equation can be obtained directly, which showed many advantages *versus* the sequential refinement, as long as a physically meaningful model is used. It is more accurate and sensitive to lower weight fraction concentration (Müller *et al.*, 2009).

Here we present the solid-state $[4\pi + 4\pi]$ photodimerization reaction of 9-MA (Fig. 1). Turowska-Tyrk & Trzop (2003) reported the structural transformations in a single crystal during photodimerization. Due to the single-crystal disintegration, the reaction was limited to 28% completion. Takegoshi *et al.* (1998) showed that the reaction takes place at defects of the crystal in the monomer phase. Therefore, comprehensive knowledge of the solid-state reaction kinetics is needed. The aim of the present study is to obtain the kinetics parameters of the crystalline 9-MA photodimerization of bulk material at a much higher level of completion using the JMAK equation.

2. Experimental

9-MA powder (98% pure; Wako Chemical Co., Japan) was purified by recrystallization from acetone and hexane solvents, and then was ground by hand in an agate mortar and pestle.

X-ray powder diffraction measurements: The experiment was performed at the X-ray time-resolved beamline (NW14A) at the Photon Factory Advanced Ring (PF-AR), KEK, Japan, which has double undulators (U36 and U20) with different period lengths, covering an energy range of 5–25 keV of different harmonics. Details of the beamline have been reported previously (Nozawa *et al.*, 2007). The X-ray beam was set to an energy of 18.0 keV ($\lambda = 0.689$ Å). Approximately 1–2 mg of samples were filled into borosilicate glass capillaries (Hilgenberg, Germany) with a diameter of 0.4 mm, and mounted on a horizontal phi axis with the sample spun for better counting statistics. Debye–Scherrer powder rings were collected at room temperature using a Mar165 CCD detector with 2048 × 2048 pixels and 80 µm × 80 µm pixel size. The sample-to-detector distance was set to 150 mm.

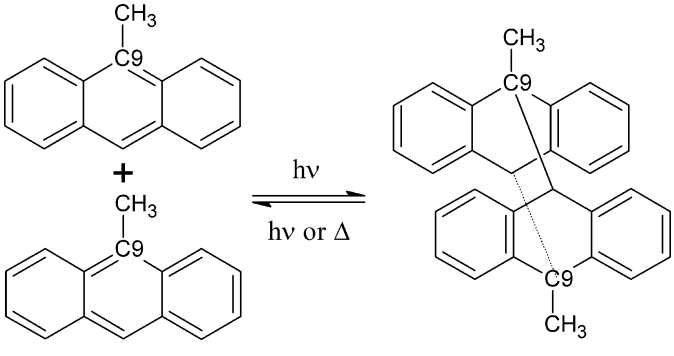

Figure 1
Photodimerization diagram of 9-MA.

The photodimerization reaction was triggered *in situ* by a Xenon lamp, equipped with a visible mirror module (385–740 nm; MAX-301, 300 W; Asahi Spectra). The temperature was measured to be ~ 303 K and the radiation power was ~ 24 mW mm^{-2} at the sample position.

The UV–vis absorption spectra were taken using a Varian Cary 50 Conc spectrophotometer in a cyclohexane solution. IR spectra were recorded on a Shimadzu IR Prestige-21 FTIR spectrometer by dispersing samples in KBr pellets.

3. Data analysis

The powder diffraction rings were converted to the standard one-dimensional data profile (2θ *versus* intensity) using *Fit*2D; the beam centre shadows were masked and the *Fit*2D geometrical correction was applied (Hammersley *et al.*, 1996). The sample-to-detector distance was calibrated by a standard Si powder to be 148.9 mm. The data presentation was carried out using *WinPLOTR* (Roisnel & Rodríguez-Carvajal, 2000) and *Powder*3D (Hinrichsen *et al.*, 2006).

3.1. Kinetic analysis based on the JMAK equation

The progress of a phase transformation reaction can be described by several steps: initially small domains of the product phase are formed within the parent phase, which is called nucleation. Nucleation can be heterogeneous if it occurs at specific locations in the parent phase, such as crystal defects, or homogeneous if its occurrence is simultaneous in the entire volume of the parent phase.

In order to understand the nature of the kinetics, information about the behaviour of nucleation and growth with time is needed (Jena & Chaturvedi, 1992). The *JMAK* model was developed by Johnson & Mehl (1939), Avrami (1939) and Kolmogorov (1937), and is widely used to describe the kinetics of different reactions. These transformations often follow a characteristic s-shaped or sigmoidal curve. The JMAK equation for an isothermal transformation can be written as

$$x(t) = 1 - \exp(-(kt)^n) \quad (1)$$

and equivalently by

$$\ln(-\ln(1 - x)) = n \ln(t) + n \ln k. \quad (2)$$

A plot of equation (2) is called a Sharp–Hancock plot (Hancock & Sharp, 1972) and yields a straight line with a slope that is equal to n and an intercept equal to $n \ln (k)$, where t is time and $x(t)$ is the evolved fraction of the product phase, k

(s^{-1}) is the reaction rate constant and n is the Avrami exponent. A comprehensive review of the development and derivation of this equation can be found elsewhere (Christian, 1981).

In general, the value of k depends on the nucleation and growth rates and is sensitive to temperature. The Avrami exponent n, the order of the reaction, describes the dimensionality of the growth of the product phase; n in the original model should be an integer number between 1 and 4, where $3 \leq n \leq 4$ for polyhedral or three-dimensional growth, $2 \leq n \leq 3$ for plate-like or two-dimensional growth and $1 \leq n \leq 2$ for one-dimensional growth, like rods or needles. Fractions and half integer values have been reported in many cases with successful interpretation (Lopes-da-Silva & Coutinho, 2007; Bertmer *et al.*, 2006; Kim *et al.*, 2005).

The Avrami exponent n is described by equation (3) (Starink, 1997; Müller *et al.*, 2009), where $N_{\rm dim}$ is the dimensionality of the crystal growth, g relates to the mechanism of growth with the value 1 for linear growth (interface-controlled process) or 1/2 for a diffusion-controlled process. B refers to the nucleation rate and is 0 in the case of site saturation (no nucleation during the transformation), $B = 1$ for continuous nucleation (at constant nucleation rate), $B > 1$ for an increasing nucleation rate, and $B < 1$ for a decreasing nucleation rate

$$n = N_{\rm dim}\, g + B. \tag{3}$$

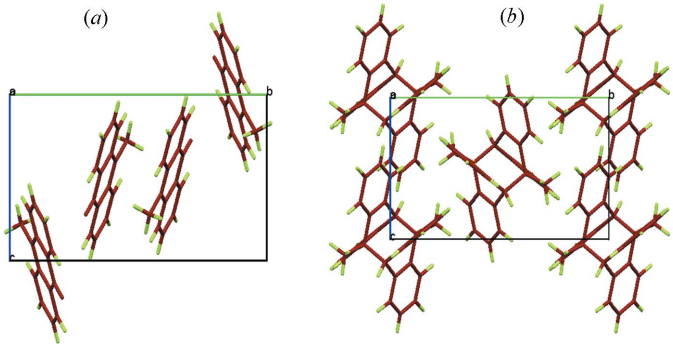

Figure 2
Crystal structure of (*a*) the 9-MA monomer phase and (*b*) the 9-MA dimer phase.

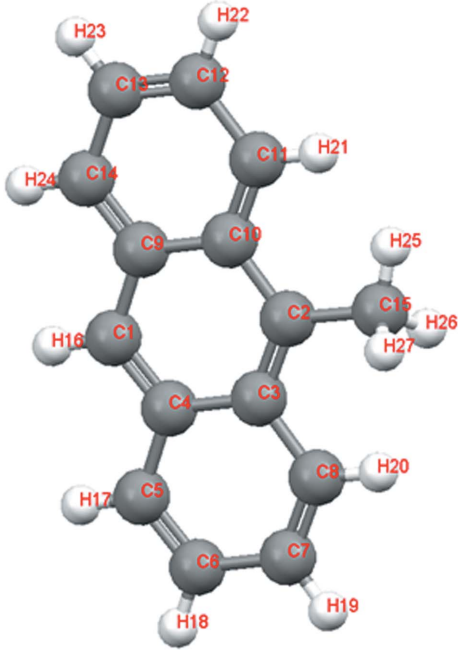

Figure 3
Rigid body of the monomer molecule.

3.2. Parametric refinement

Quantitative Rietveld refinements were performed using the *TOPAS* software in launch mode (Bruker AXS, 2009). For the refinements the monomer and the dimer molecules (Fig. 2) were given in the form of rigid bodies (Figs. 3 and 4) in *z*-matrix notation which were generated using CIFs (Turowska-Tyrk & Trzop, 2003). The orientation of the rigid bodies was determined and refined using patterns with a high amount of a particular phase and then kept constant for further refinements.

In order to compensate orientational effects of the powder, a spherical harmonics function of the order four was used for each phase. Apart from that lattice parameters were refined. In the case of the monomer phase the crystallite size was also refined using the same value for Lorentzian and Gaussian fractions in each pattern. As a first step, traditional sequential Rietveld refinements were performed. Results showed that the evolution of the phases can be described using the JMAK equations (1) and (2). This fact was used in parametric Rietveld refinement. In that case the scale factor was parameterized using the JMAK equation to describe the emergence of the dimer phase, as shown in equation (4); details about this equation can be found in Müller *et al.* (2009).

$$S_{\rm m} = \frac{-S_{\rm d} M_{\rm d} V_{\rm d} [\exp(-k(t)^n)]}{M_{\rm m} V_{\rm m} [\exp(-k(t)^{\rm n}) - 1]}, \tag{4}$$

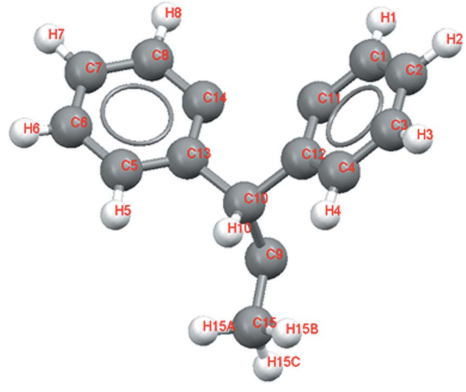

Figure 4
Rigid body of the dimer molecule. Due to symmetry constraints only one half of the molecule is necessary within the rigid body. The remaining part of the molecule is generated by symmetry.

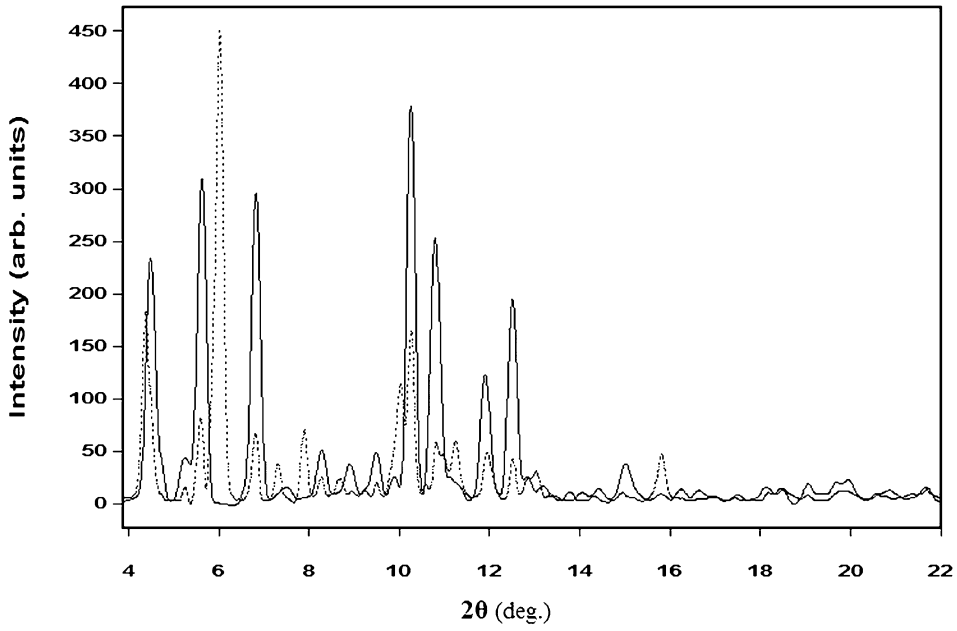

Figure 5
Powder patterns of 9-MA before the photo-excitation (solid line) and after 9 h of illumination (dotted line).

where S_m is the scale factor of the monomer phase, S_d the scale factor of the dimer phase, k and n are parameters of the JMAK equations (2) and (3), M_d is the mass of unit cells of the dimer phase and M_m of the monomer phase, V_d and V_m are the volumes of the unit cells of the dimer and monomer phases, respectively, and t is the exposure time. In the parametric refinement for both phases the same parameters were refined as in the previous sequential refinement. The values of n and k can most easily be obtained using a Sharp–Hancock plot (Hancock & Sharp, 1972). An example of an input file of parametric Rietveld refinement can be found in the supplementary information. The experimental details are given in Table 1[1]

4. Results and discussion

The powder patterns obtained from *in situ* photoexcitation of a 9-MA sample show the appearance of the 9-MA dimer phase (Fig. 5). Quantitative phase analysis was performed using the structural parameters from a single-crystal refinement (Turowska-Tyrk & Trzop, 2003).

UV–vis and IR spectroscopic results for the illuminated sample also indicate the presence of the 9-MA dimer (Fig. 6). UV–vis spectra showed the disappearance of the absorption peaks of the monomer phase between 350 and 400 nm as shown in Fig. 6(*a*), which can be considered as an indicator for the formation of the dimer phase (Tillman *et al.*, 2007). A comparison of IR measurements of the original and the illuminated sample shows that the band at 884 cm^{-1} is missing in the illuminated one as shown in Fig. 6(*b*). This is caused by the 9,10-substitution during the dimerization process (Singh & Sandorfy, 1969).

Fig. 7 shows the time-resolved three-dimensional plots of the diffraction patterns. Fig. 8 illustrates the propagation of a typical Bragg diffraction peak during the photoreaction. Dimer peaks start to appear clearly after 30 min. The distinctive peak of the dimer phase around 2θ (6°) starts to increase noticeably with time.

More accurate and specific interpretation was given by the quantitative Rietveld refinements. In Fig. 9 an example of the Rietveld refinement is given. Fig. 10 shows a comparison of the evolution of the weight fraction for the monomer and dimer phases with time. The results of sequential and

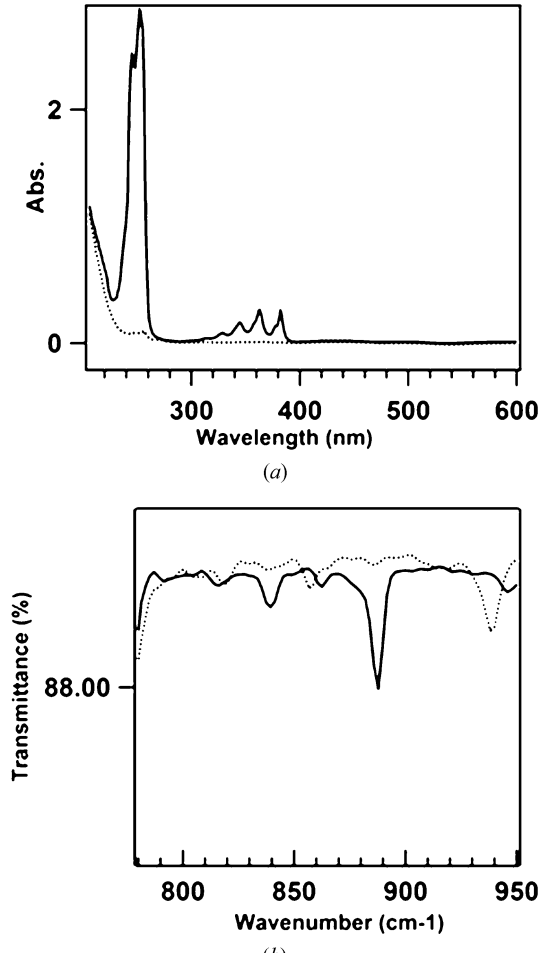

Figure 6
(*a*) UV–vis spectrum of 9-MA (solid line) and the irradiated sample (dotted line). (*b*) The selected range of the IR spectra of 9-MA shows the disappearance of the band at 884 cm^{-1} for the illuminated sample (dotted line).

[1] Supplementary data for this paper are available from the IUCr electronic archives (Reference: KD5063

Table 1
Experimental details.

For all structures: monoclinic, $P2_1/c$. Experiments were carried out at 303 K with synchrotron radiation, λ = 0.689 Å using a MarDTB diffractometer at NW14A beamline. Refinement was on 37 parameters.

	Monomer phase	Dimer phase
Crystal data		
Chemical formula	$C_{15}H_{12}$	$C_{30}H_{24}$
M_r	192.25	384.49
a, b, c (Å)	8.679 (3), 14.402 (3), 8.026 (2)	9.851 (2), 13.285 (3), 8.1301 (17)
β (°)	96.95 (3)	115.14 (2)
V (Å^3)	995.8 (5)	963.2 (4)
Z	4	2
Specimen shape	Cylinder	Cylinder
Data collection		
Specimen mounting	Capillary	Capillary
Data collection mode	Transmission	Transmission
Scan method	Fixed	Fixed
2θ values (°)	$2\theta_{min}$ = 0, $2\theta_{max}$ = 30, $2\theta_{step}$ = 0.0146	$2\theta_{min}$ = 0, $2\theta_{max}$ = 30, $2\theta_{step}$ = 0.0146
Refinement		
R factors and goodness-of-fit	R_p = 2.50, R_{wp} = 3.28, R_{exp} = 10.133, χ^2 = 0.109	R_p = 2.50, R_{wp} = 3.28, R_{exp} = 10.133, χ^2 = 0.109
No. of data points	1707	1707

Table 2
Comparison of Avrami constants 'n' and 'k' as obtained directly from the parametric refinement results and using a fit of the Sharp–Hancock plot for sequential refinement (Fig. 9).

	n	k (s^{-1})	R_{wp}
Parametric refinement	0.599 (4)	2.97 (3) × 10^{-5}	3.29
Sequential refinement	0.618 (7)	3.02 (5) × 10^{-5}	2.84–5.62

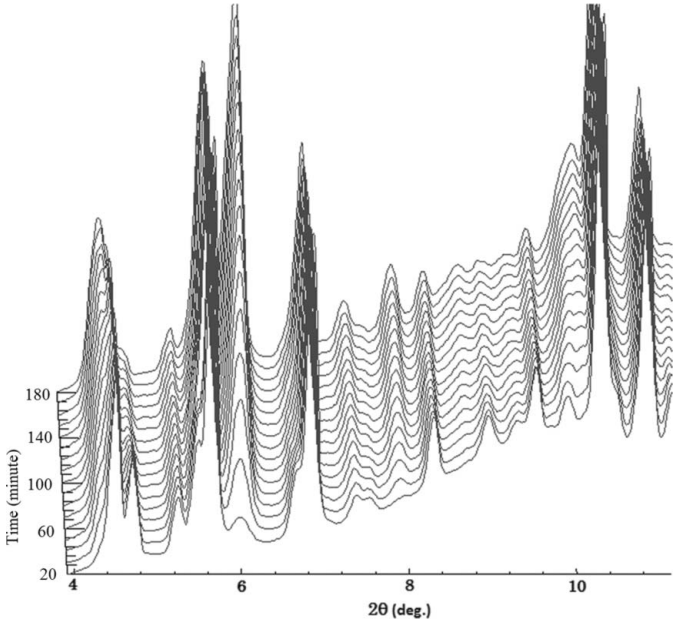

Figure 7
Three-dimensional plot showing a cut out of the time-resolved three-dimensional plot of the diffraction patterns.

parametric refinements show good agreement. The dimer fraction reached 63.87 wt % after 9 h.

The curve of photodimerization (Fig. 10) suggests that the JMAK model is applicable to describe this transformation. Additionally, other experiments in the literature showed similar curves for 9-MA dimerization (see Takegoshi *et al.*, 1998). It is notable in the plot of the parametric refinement results (Figs. 10 and 11) that all the points are compelled to lie on the JMAK model function.

Table 2 gives a comparison of Avrami constants 'n' and 'k' as obtained directly from the parametric refinement results and using a fit of the Sharp–Hancock plot for sequential refinement (Fig. 11). The difference in n values is within experimental error. This suggests the following kinetic model: one-dimensional diffusion-controlled growth with a decreasing rate, and heterogeneous nucleation.

We interpreted our data based on the JMAK model. It was noted that the Avrami parameter n can be smaller than 1 (Kim *et al.*, 2005; Todinov, 1996; Starink, 1997), which might indicate the nucleation rate was decreasing with reaction time, which was reported in similar cases, for instance in the photodimerization of α-*trans*-cinnamic acid (Bertmer *et al.*, 2006).

Hulbert (1969) reported that the Avrami exponent n can vary between 0.5 and 1.5 in the case of one-dimensional diffusion-controlled reactions, n is close to 0.5 for instantaneous nucleation and close to 1.5 if the nucleation rate is constant. Applying our suggested kinetic model to equation

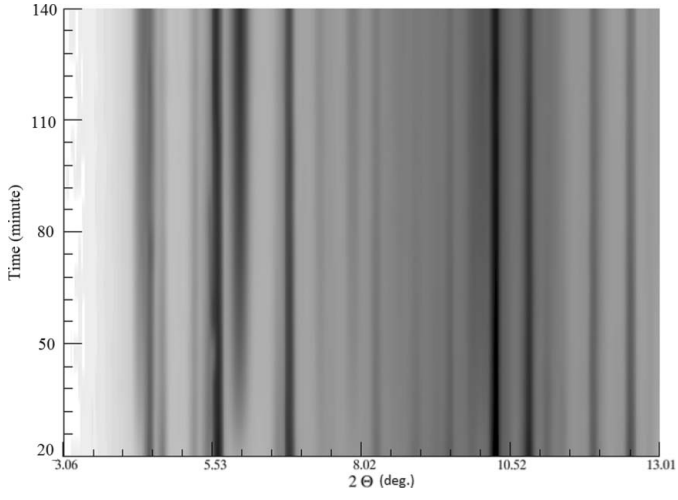

Figure 8
Waterfall presentation of the propagation of typical Bragg diffraction peaks. Shows the most prominent peak of the dimer phase (2θ = 6°).

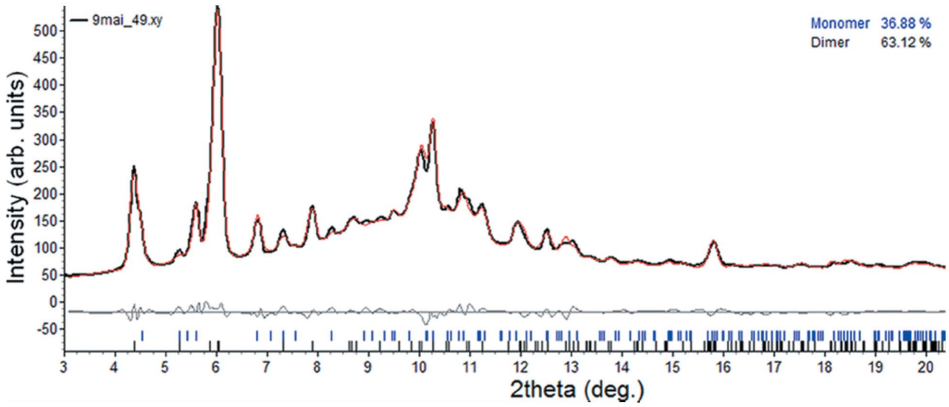

Figure 9
Rietveld plot of the full quantitative Rietveld refinement of 9-MA transformation from the monomer to the dimer phase after 9 h (9mai_49).

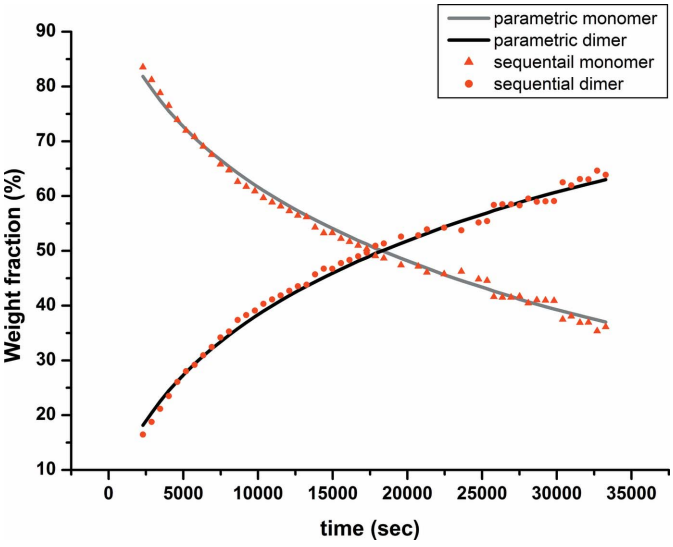

Figure 10
Comparison of the weight fraction progress with time obtained for the monomer and dimer phase in sequential and parametric Rietveld refinement.

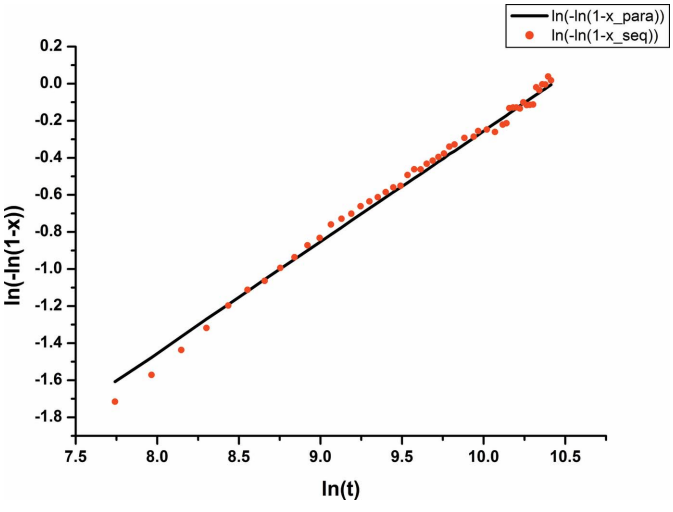

Figure 11
Comparison of the Sharp–Hancock plot of the values obtained in sequential and parametric Rietveld refinement.

(3) shows agreement between the obtained values of n (Table 2) and the result of Hulbert (1969), which can be rationalized as follows: In our case N_{dim} is equal to 1 for one-dimensional growth, while $g = 0.5$ for a diffusion-controlled process and $B < 1$, which indicates a decreasing nucleation rate. Substitution of these values in equation (3) gives $0.5 + (B < 1) = n$, which indicates that the equation would be correct for $0.5 < n < 1.5$. This agrees with the n values obtained (Table 2).

Photodimerization often has a heterogeneous character (Moré *et al.*, 2010). It was mentioned (Lopes-da-Silva & Coutinho, 2007; Sperling, 1992; Keith & Padden, 1964) that the rather low values of n refer to heterogeneous nucleation, which can be explained as a result of nucleation at crystal defects such as grain boundaries, dislocations or stacking faults (Jena & Chaturvedi, 1992). In addition, Wernick & Schochet (1988) and Takegoshi *et al.* (1998) showed that the dimerization of 9-substituted anthracene is initiated at crystal-defect sites and is not a homogenous process.

Based on the above-mentioned discussion we summarize our suggested model for the kinetics of the 9-MA photodimerization reaction as follows. The reaction starts by the absorption of light in the parent phase (monomer) to initiate nucleation of the dimer phase. The required free energy for the nucleation process varies with different crystal locations and those possessing the least energy are the preferential sites, so the defect locations are preferred (Jena & Chaturvedi, 1992). Once the nuclei of the product phase are formed, the progress of the growth takes place controlled by the rate at which the atoms diffuse in the parent phase. With ongoing illumination the nuclei of the dimer phase grow and consequently the fraction of the dimer phase increases while the fraction of the untransformed phase decreases.

5. Conclusion

We performed a time-resolved X-ray powder diffraction study of 9-methylanthracene during $[4\pi + 4\pi]$ photodimerization, which is a typical example of a solid-state photodimerization reaction, and has previously been studied using single crystals (Turowska-Tyrk & Trzop, 2003). The study overcomes the drawbacks of single crystals by the application of powder diffraction, taking advantage of fast full quantitative parametric Rietveld refinement of bulk material using CCD area detectors and synchrotron light.

The JMAK model can give valuable information about phase transformation kinetics, which can be extracted directly from parametric Rietveld refinement with high accuracy.

The suggested kinetic model for 9-MA photodimerization comprises a heterogeneous decreasing nucleation which is followed by diffusion-controlled growth.

This study was supported by a Short-stay Program Studying Abroad FY2011 grant of the Graduate University for Advanced Studies (Sokendai), Japan. We thank Dr Michael Cheah [Australian National Beamline Facility (ANBF), KEK, Japan] for his help of spectroscopic measurements. The synchrotron X-ray experiment at KEK was approved by the Photon Factory Program Advisory Committee (PF-PAC No. 2004S2-001).

References

Avrami, M. (1939). *J. Chem. Phys.* **7**, 1103–1112.
Bell, P. R. (1948). *Phys. Rev.* **73**, 1405–1406.
Benedict, J. B. & Coppens, P. (2009). *J. Phys. Chem. A*, **113**, 3116–3120.
Bertmer, M., Nieuwendaal, R. C., Barnes, A. B. & Hayes, S. E. (2006). *J. Phys. Chem. B*, **110**, 6270–6273.
Bouas-Laurent, H., Castellan, A., Desvergne, J. P. & Lapouyade, R. (2000). *Chem. Soc. Rev.* **29**, 43–55.
Bratschkov, C., Karpuzova, P., Müllen, K., Klapper, M. & Schopov, I. (2001). *Polym. Bull.* **46**, 345–349.
Bruker AXS (2009). *TOPAS*, Version 4.2. Bruker AXS, Karlsruhe, Germany.
Christian, J. W. (1981). *The Theory of Transformations in Metals and Alloys*, pp 525–548. Oxford: Pergamon Press.
Dvornikov, A. S. & Rentzepis, P. M. (1996). *Res. Chem. lntermed.* **22**, 115–128.
Feringa, B. L., van Delden, R. A., Koumura, N. & Geertsema, E. M. (2000). *Chem. Rev.* **100**, 1789–1816.
Hammersley, A. P., Svensson, M., Hanfland, M., Fitch, A. N. & Haeussermann, D. (1996). *High Press. Res.* **14**, 235–248.
Hancock, J. D. & Sharp, J. H. (1972). *J. Am. Ceram. Soc.* **55**, 74–77.
Harris, K. D. M., Tremayne, M., Lightfoot, P. & Bruce, P. G. (1994). *J. Am. Chem. Soc.* **116**, 3543–3547.
Hinrichsen, B., Dinnebier, R. E. & Jansen, M. (2006). *Z. Kristallogr.* Suppl. **23**, 231–236.
Hulbert, S. F. (1969). *J. Br. Ceram. Soc.* **6**, 11–20.
Jena, A. K. & Chaturvedi, M. C. (1992). *Phase Transformations in Materials.* New Jersey: Prentice-Hall.
Johnson, W. A. & Mehl, P. A. (1939). *Trans. AIME*, **135**, 416–441.
Keith, H. D. & Padden, F. J. (1964). *J. Appl. Phys.* **35**, 1270–1285.
Kim, J. H., Jaung, J. Y. & Jeong, S. H. (2003). *Opt. Mater.* **21**, 395–400.
Kim, S., Kim, W. K., Kaczynski, R. M., Acher, R. D., Yoon, S., Anderson, T. J., Crisalle, O. D., Payzant, E. A. & Li, S. S. (2005). *J. Vac. Sci. Technol. A*, **23**, 310–315.
Kolmogorov, A. N. (1937). *Bull. Acad. Sci. USSR Phys. Ser.* **1**, 355–359.
Lopes-da-Silva, J. A. & Coutinho, J. A. P. (2007). *Energy Fuels*, **21**, 3612–3617.
Madsen, I. C. & Scarlett, N. Y. (2008). *Powder Diffraction – Theory and Practice*, edited by R. E. Dinnebier & S. J. L. Billinge, pp. 298–331. Cambridge: Royal Society of Chemistry, Cambridge Press.
Molard, Y., Bassani, D. M., Desvergne, J.-P., Moran, N. & Tucker, J. H. R. (2006). *J. Org. Chem.* **71**, 8523–8531.
Moré, R., Busse, G., Hallmann, J., Paulmann, C., Scholz, M. & Techert, S. (2010). *J. Phys. Chem. C*, **114**, 4142–4148.
Müller, M., Dinnebier, R. E. & Jansen, M. (2009). *Powder Diffr.* **24**, 191–199.
Nozawa, S., Adachi, S., Takahashi, J., Tazaki, R., Guérin, L., Daimon, M., Tomita, A., Sato, T., Chollet, M., Collet, E., Cailleau, H., Yamamoto, S., Tsuchiya, K., Shioya, T., Sasaki, H., Mori, T., Ichiyanagi, K., Sawa, H., Kawata, H. & Koshihara, S. (2007). *J. Synchrotron Rad.* **14**, 313–319.
Roisnel, T. & Rodríguez-Carvajal, J. (2000). *WinPLOTR. Proceedings of the Seventh European Powder Diffraction Conference* (EPDIC 7), pp. 118–123, edited by R. Delhez & E. J. Mittemeijer. 20–23 May, Barcelona, Spain.
Schmidt, G. M. J. (1971). *Pure Appl. Chem.* **27**, 647.
Singh, S. & Sandorfy, C. (1969). *Can. J. Chem.* **47**, 257–263.
Sperling, L. H. (1992). *Introduction to Physical Polymer Science*, 2nd ed., pp. 234–238. Wiley and Sons: New York.
Starink, M. J. (1997). *J. Mater. Sci.* **32**, 4061–4070.
Stinton, G. W. & Evans, J. S. O. (2007). *J. Appl. Cryst.* **40**, 87–95.
Svensson, S. O., Birch, J., Müller, H. & Kvick, Å. (1997). *J. Synchrotron Rad.* **4**, 83–94.
Takegoshi, K., Nakamura, S. & Terao, T. (1998). *Solid State Nucl. Magn. Reson.* **11**, 189–196.
Tillman, E. S., Miller, D. J. & Roo, A. C. (2007). *Polym. Bull.* **58**, 881–891.
Todinov, M. T. (1996). *Acta Mater.* **44**, 4697–4703.
Tsudera, T., Ikeda, A. & Shinkai, S. (1997). *Tetrahedron*, **53**, 13609–13620.
Turowska-Tyrk, I. (2004). *J. Phys. Org. Chem.* **17**, 837–847.
Turowska-Tyrk, I. & Trzop, E. (2003). *Acta Cryst.* B**59**, 779–786.
Wernick, D. L. & Schochet, S. (1988). *J. Phys. Chem.* **92**, 6773–6778.